

Calibration of Partially-Fixed Viewpoint Active Camera

JUNJI KONDOU[†], XIAOJUN WU[†], TAKASHI MATSUYAMA^{††}

The fixed viewpoint (FV) camera, whose projection center stays fixed irrespectively of any camera rotations, enables us to capture very high resolution omni-directional panoramic images as well as facilitates active object tracking in a wide spread area^{1),2)}. From an engineering point of view, however, it is hard to develop a very accurate, i.e. of pixel-wise accuracy, FV camera; while it is not difficult to align a pair of (pan and tilt) rotation axes to intersect at right, the accurate determination of the projection center and its precise alignment at the intersection point require very elaborated works. Moreover, zooming, which shifts the projection center, easily damages the fixed viewpoint property.

To develop an easily realizable FV camera, we propose a practical FV camera model named *partially-fixed viewpoint* (PFV) camera, whose projection center is encased in a limited volume around the rotation center. In this paper, giving a sophisticated camera model for the PFV camera, we conduct extensive experiments for its calibration and analyze characteristics of the employed camera parameters. Then we propose a method that enables us to use a PFV camera as an FV camera. Our basic idea is that 1. Partition the full rotation range into a group of sub-ranges. 2. In each sub-range, determine the camera parameters that enables a PFV camera to be used as an FV camera. 3. Finally, integrate all calibration processes for the sub-ranges so that we can use a PFV camera as an FV camera in the full range of rotation. Experimental results show the effectiveness of the proposed method.

1. Introduction

To obtain the object's geometry information from an image is quite a basic task in tracking, recognition, and other computer vision applications. Usually, we do this by establishing a projection model. Based on the model, we can relate the pixel on an image to the object in the real world. This is known as the calibration of a camera.^{3),6),7)} Generally, comparing with fixed cameras, calibration of active cameras is complex because not only a projection model but also a motion model is necessary. To simplify the calibration, we have proposed a model as the *fixed viewpoint* (FV) camera¹⁾, whose viewpoint is fixed on the rotation center of a pan-tilt unit(PTU). We have also developed the FV active camera. Since the viewpoint is fixed while the camera's moving, the FV camera enables us to capture very high resolution omni-directional panoramic images as well as facilitates active object tracking in a wide spread area^{2),4),5)}. In spite of the efficiency, from an engineering point of view, it is hard to develop a very accurate, i.e. of pixel-wise accuracy, FV camera; while it is not difficult to align a pair of (pan and tilt) rotation axes to intersect at right, the accurate determination of the projection center and its

precise alignment at the intersection point require very elaborated works. Moreover, zooming, which shifts the projection center, easily damages the fixed viewpoint property⁸⁾.

To develop an easily realizable FV camera, we propose a practical FV camera model named *partially-fixed viewpoint* (PFV) camera, whose projection center is encased in a limited volume around the rotation center. In this paper, we propose a calibration method for such a PFV camera. By the method, we can utilize a PFV camera as the FV camera. Our ideas are shown as the following:

- (1) We can use a PFV camera as the FV camera within a limited rotary range. Because the projection center is in a limited distance from the rotation center, the parallax can be observed only when the camera rotates over a broad range. That is to say, there exists a sub-range of rotation within which the parallax cannot be observed. Within such a sub-range, we can calibrate a PFV camera as the FV one.
- (2) For a wide rotary range, we can partition the full rotary range into sub-ranges within the limitation mentioned above. We can calibrate the camera as the FV camera for each sub-range. And by integrating all the calibration processes, we can realize the FV camera over the full

[†] Department of Intelligent Science and Technology,
 Graduate School of Informatics, Kyoto University

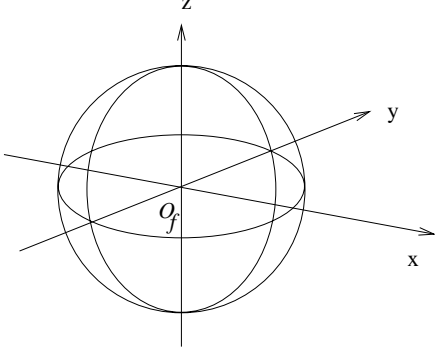


Fig. 1 PTU Coordinate System

rotary range.

In the following sections, we first describe a projection model and the concrete method for calibrating a PFV camera as the FV camera. Experimental results are shown to estimate the precision of the method. Second, we describe a method for the measurement of the gap between the projection center and the rotation center. We then can determine the limitation of the sub-range for a wide rotary range to be partitioned. Finally, we show a concrete integration method for all calibration processes of the sub-ranges. Also some experimental results are shown to prove the the effectiveness of the proposed PFV model and the methods.

2. Calibration as The FV Active Camera

In this section, we describe the calibration method of a PFV as the FV camera. The PFV camera is assumed to have two rotation axes (pan and tilt). Also the rotary range is assumed to be narrow enough for no parallax being observed.

2.1 PTU Coordinate System

Firstly, we define the PTU coordinate system \mathcal{C}_{PTU} as shown in Figure 1. The origin is on the rotation center of the PTU. The Y-axis is in the viewing direction of the camera when PTU's pan and tilt are 0. The XY-plane is vertical to the pan rotation axis. The direction of the camera can then be represented as a vector from the origin. Due to the installation error, the direction of the camera differs from the direction of the PTU. To correct camera direction, we introduce the parameter T_{off} to represent the offset angle in tilt.(Figure 2).

2.2 Projection Model

Our projection model is based on the perspective projection shown in Figure 2. The pro-

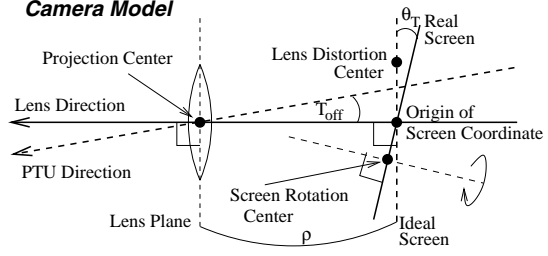


Fig. 2 Projection Model

jection center is the origin of \mathcal{C}_{PTU} . And the screen is placed vertically to the viewing direction in a distance of the focal length(ρ). To distinguish the screen from a real screen, we note it as the ideal screen. On the ideal screen, we define a 2D coordinate system \mathcal{C}_{ideal} . The origin is at the intersection point of the viewing direction and the screen. The X-axis is parallel with the XY-plane of the \mathcal{C}_{PTU} .

Due to kinds of distortion in practice, we introduce the following models to compensate the plain perspective projection model.

First, the lens distortion effects the coordinates on the ideal screen. And it can be modeled by the following radial distortion:

$$\begin{pmatrix} {}^{id}x_d \\ {}^{id}y_d \end{pmatrix} = \begin{pmatrix} {}^{id}x_u - {}^{id}O_x \\ {}^{id}y_u - {}^{id}O_y \end{pmatrix} (1 + \kappa R^2) + \begin{pmatrix} {}^{id}O_x \\ {}^{id}O_y \end{pmatrix} \quad (1)$$

$R^2 = ({}^{id}x_u - {}^{id}O_x)^2 + ({}^{id}y_u - {}^{id}O_y)^2$ where κ is the distortion factor and $({}^{id}O_x, {}^{id}O_y)$ is the radial distortion center. Point $({}^{id}x_u, {}^{id}y_u)$ on the ideal screen is mapped to $({}^{id}x_d, {}^{id}y_d)$ by the lens distortion.

Next, due to the installation error, the position of the real screen may differ from that of the ideal screen. We define a new 2D coordinate system \mathcal{C}_{real_r} to represent the real screen. The real screen is modeled by the following two-step rotations of the ideal screen.

- (1) We define the coordinate system \mathcal{C}_{real_t} for the screen after the first step rotations. The origin of \mathcal{C}_{real_t} is same as \mathcal{C}_{ideal} . The X-Axis of \mathcal{C}_{real_t} is positioned by rotating the X-Axis of \mathcal{C}_{ideal} θ_P on the Y-Axis of \mathcal{C}_{ideal} . And then, the Y-Axis of \mathcal{C}_{real_t} is positioned by rotating the Y-Axis of \mathcal{C}_{ideal} θ_T on the X-Axis of \mathcal{C}_{real_t} . The point on the ideal screen $({}^{id}x_d, {}^{id}y_d)$ is then mapped

to the coordinates $({}^{\text{re}}x_t, {}^{\text{re}}y_t)$ in $\mathcal{C}_{\text{real}_t}$. $({}^{\text{re}}x_t, {}^{\text{re}}y_t)$ can be calculated as below:

$$\begin{pmatrix} {}^{\text{re}}x_t \\ {}^{\text{re}}y_t \end{pmatrix} = \rho_s \frac{A \begin{pmatrix} \text{id } x_d \\ \rho \\ \text{id } y_d \end{pmatrix}}{D_s^T \begin{pmatrix} \text{id } x_d \\ \rho \\ \text{id } y_d \end{pmatrix}} - \rho \begin{pmatrix} \sin \theta_P \\ \sin \theta_T \cos \theta_P \end{pmatrix} \quad (2)$$

$$A = \begin{pmatrix} \cos \theta_P & -\sin \theta_P \\ -\sin \theta_T \sin \theta_P & -\sin \theta_T \cos \theta_P \\ 0 & \cos \theta_T \end{pmatrix}$$

$$\rho_s = \rho \cos \theta_T \sin \theta_P$$

$$D_s = \begin{pmatrix} \cos \theta_T \sin \theta_P \\ \cos \theta_T \cos \theta_P \\ \sin \theta_T \end{pmatrix}$$

- (2) The second step is a rotation on the same screen as $\mathcal{C}_{\text{real}_t}$ defines. The rotation center is ${}^{\text{re}}O$ in $\mathcal{C}_{\text{real}_t}$. The rotation angle is φ . Then the coordinates $({}^{\text{re}}x_r, {}^{\text{re}}y_r)$ on the real screen can then be transformed from $({}^{\text{re}}x_t, {}^{\text{re}}y_t)$ in $\mathcal{C}_{\text{real}_t}$ as below:

$$\begin{pmatrix} {}^{\text{re}}x_r \\ {}^{\text{re}}y_r \end{pmatrix} = \begin{pmatrix} \cos \varphi & \sin \varphi \\ -\sin \varphi & \cos \varphi \end{pmatrix} \begin{pmatrix} {}^{\text{re}}x_t - {}^{\text{re}}O_x \\ {}^{\text{re}}y_t - {}^{\text{re}}O_y \end{pmatrix} + \begin{pmatrix} {}^{\text{re}}O_x \\ {}^{\text{re}}O_y \end{pmatrix} \quad (3)$$

Finally, we introduce the aspect ratio α and the coordinates of OSC (${}^{\text{im}}O_x, {}^{\text{im}}O_y$) to map the pixels on the input image to the points on the real screen. The OSC is the mapped position of the origin of $\mathcal{C}_{\text{real}_r}$ on the input image. The point $({}^{\text{re}}x_r, {}^{\text{re}}y_r)$ on the real screen is mapped to the point $({}^{\text{im}}x, {}^{\text{im}}y)$ on the input image as below:

$$\begin{pmatrix} {}^{\text{re}}x_r \\ {}^{\text{re}}y_r \end{pmatrix} = \begin{pmatrix} ({}^{\text{im}}x - {}^{\text{im}}O_x)/\alpha \\ \text{size}_y - ({}^{\text{im}}y - {}^{\text{im}}O_y) \end{pmatrix} \quad (4)$$

where size_y is the vertical size of the image.

Based on the projection model, we can define the set of camera parameters Ψ as

$$\Psi^T = (\rho, T_{\text{off}, o}, {}^{\text{im}}O_x, {}^{\text{im}}O_y, \kappa, \text{id } O_x, \text{id } O_y, \theta_P, \theta_T, \varphi, {}^{\text{re}}O_x, {}^{\text{re}}O_y, \alpha) \quad (5)$$

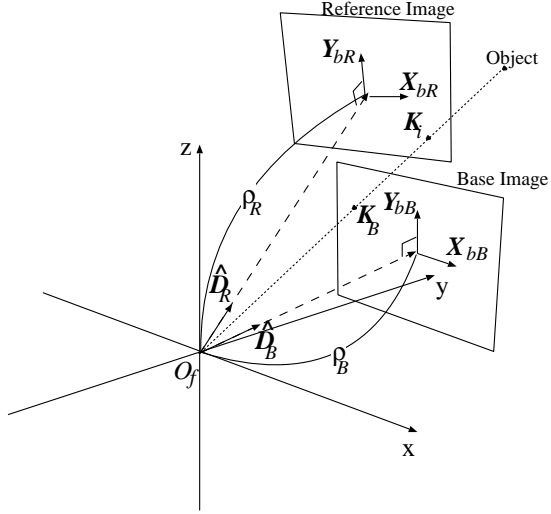


Fig. 3 Calibration Algorithm

The calibration is equal to deriving an optimal Ψ and the algorithm is described below.

2.3 Calibration Algorithm

As for an FV active camera, there exists no parallax on images acquired in different directions. So we can generate one seamless image by projecting these images to one virtual screen. Conversely, estimating the quality of the generated image provides us hand-holds to find the correct Ψ . To distinguish these images in different directions, we call one of them as “Base Image”. The rest other images are called as “Reference Image”. As shown in Figure 3, the viewing angle of “Base Image” and “Reference Image” overlap each other. The point K_B is related to K_i as they are projected by the same object in the real world. We define the angle

$$e = \angle K_B O_f K_i \quad (6)$$

as the error function. K_B and K_i are called as a pair of *related feature points*. In theory, e should be 0 when the parameter Ψ is correct. Assuming there are M pairs of related points and let \mathbf{E} be the set of all e , the calibration can be done by solving the following optimization problem:

$$\Psi = \arg \min \{S\} \quad (7)$$

$$S = \sum_{i=0}^{M-1} e_i^2, e_i \in \mathbf{E}$$

And the concrete calibration algorithm is shown as the following:

- (1) Acquire images in \mathbf{D}_B and several \mathbf{D}_i , keeping the angle of each \mathbf{l}_i overlaps with \mathbf{l}_B .

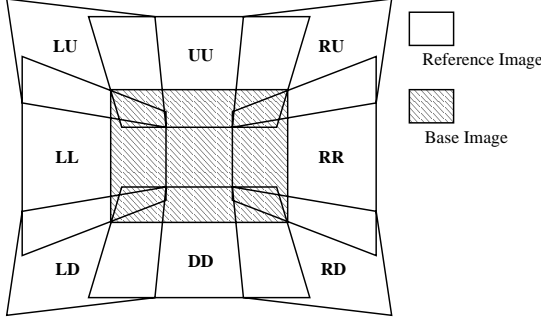


Fig. 4 Camera Work for Calibration

- (2) Select M pairs of related feature points among acquired images,
- (3) Giving an initial Ψ_0 , solve the optimization problem shown as equation(7)

To implement the above algorithm, we have to determine the camera work for calibration in the step (1). We will show evaluation experiments about the camera work for calibration in the next section.

2.4 Evaluation Experiments

2.4.1 Evaluation of Camera Work for Calibration

Determining one base viewing direction \mathbf{D}_{base} , we prepared other 8 images in 8 different directions which have equal offset from \mathbf{D}_{base} (Figure 4). We calibrated the camera by using different combination of input images. For example, selecting \mathbf{l}_L , the image on the left to \mathbf{l}_{base} , and \mathbf{l}_{base} as the input images, we got the parameter Ψ_{LL} . In like manner, we got other parameters as Ψ_{RR} , Ψ_{UU} , Ψ_{LDRU} and so on.

For each of these $\{\Psi\}$, the normalized error $\varepsilon_i = e_i \frac{1}{M} \sum_{i=0}^{M-1} e_i$ on every selected feature points was calculated. Figure 5 shows the dispersion of the ε_i in a normalized feature points space. From the figure, the error dispersion of the calibration using all of the 9 images is smallest. So the camera work of capturing in equally different directions is best for the calibration.

2.4.2 Evaluation of Projection Model

To evaluate the accuracy of the proposed projection model, we have calibrated the camera in 3 different base viewing directions. For each case, the evaluation value (\mathcal{S}) and the average error are shown in Table 1. The error in pixel is less than 1.0. That is, for each case, Ψ has accuracy to within one pixel. The proposed projection model satisfies the PFV camera well.

The angle of one pixel is measured later in Section 3 and is shown in Table 3 as τ

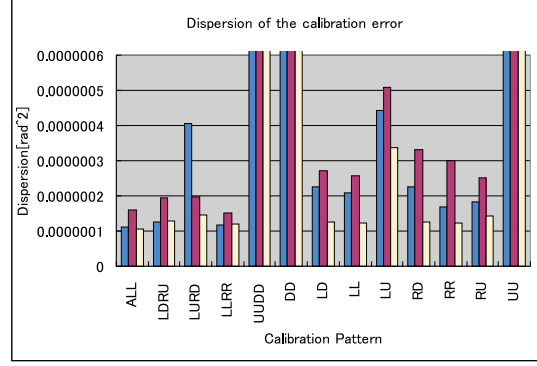


Fig. 5 Dispersion of the calibration errors

And then we are able to utilize the PFV camera as the FV camera.

Next, we show the values of Ψ for each case in Table 2. In the table, the value of each

Table 2 Evaluation Experiment

Ψ	(-15,7)	(-40,7)	(-65,7)
$\kappa[10^{-7} \text{pix}^{-2}]$	-1.001	-1.010	-0.9780
${}^{\text{id}}O_x[\text{pix}]$	278.638	318.019	294.242
${}^{\text{id}}O_y[\text{pix}]$	230.208	166.796	239.810
$\varphi[\text{deg}]$	-0.554	-0.554	-0.545
$\rho[\text{pix}]$	1028.17	1020.48	1027.18
$\theta_T[\text{deg}]$	0.130	-0.315	0.273
$\theta_P[\text{deg}]$	-0.165	-0.728	-0.340
α	0.999	1.002	1.001
${}^{\text{im}}O_x[\text{pix}]$	305.193	307.462	306.796
${}^{\text{im}}O_y[\text{pix}]$	241.670	227.191	241.827
${}^{\text{re}}O_x[\text{pix}]$	-4.442	-1.912	-1.091
${}^{\text{re}}O_y[\text{pix}]$	-9.504	-3.184	-7.099
$T_{\text{off}}[\text{deg}]$	-4.733	-4.629	-4.908

parameter changes for different cases. And the values of θ_T and θ_P changes greatest and most irregularly. We consider that the slight shift of the projection center in practice is absorbed by the parameters of θ_T and θ_P . These two parameters represent the rotations of the real screen in the model. In practice, a shift of the projection center results the change of the focal length. And the rotations of the screen in the model also result the change of the focal length. As a result, the focal length in the table changes little while the projection center of the PFV camera does shift. So we consider the shift of the projection is absorbed by the rotations of the real screen.

Among these 3 cases, the values of (1) the parameter to fit the viewing direction (T_{off}), (2) the focal length(ρ) and (3) the parameters about the lens distortion(κ , (${}^{\text{id}}O_x$, ${}^{\text{id}}O_y$)) almost keep constant. This fact allows us to find

Table 1 Average of Square of Errors at Feature Points

Base Direction (pan, tilt)[deg]	(-15,7)	(-40,7)	(-65,7)
Evaluation Value (S)	0.000418	0.000511	0.000267
Average of Error (\bar{e})[rad]	0.000651	0.000718	0.000527
Average of Error [pixel]	0.78	0.86	0.63

a proper method to integrate calibration processes for different sub-ranges, which we will describe in Section 4.

The experimental results show the proposed projection model and methods are efficient to calibrate a PFV camera as the FV camera.

3. The Limitation of Sub-range as FV cameras

We have proposed the projection model to calibrate a PFV camera as the FV camera. Experimental results prove the efficiency of the model. In this section, we will first show the measurement of the gap between the viewpoint and the rotation center. We then can determine the limitation of the rotary range to use the PFV camera as the FV camera.

3.1 The Measurement of the Gap between Viewpoint and Rotation Center

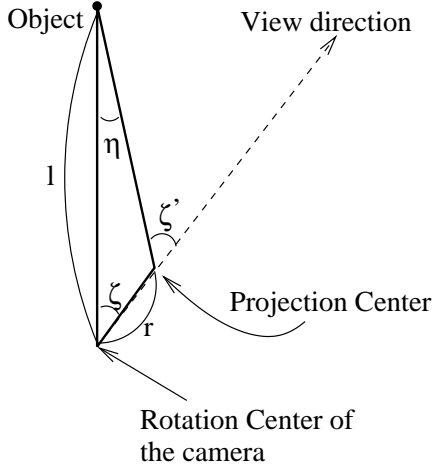


Fig. 6 Relation between Parallax and the Gap

Figure 6 shows the mechanism of parallax caused by the rotation of a camera. Here r means the gap between the viewpoint and the rotation center. We can calculate the gap r from equation (8) by measuring the distance of the object l and the angles of ζ, ζ' .

$$r = l \left(\cos \zeta - \frac{\sin \zeta}{\tan \zeta'} \right) \quad (8)$$

Because the direction of each pixel on one

image differs from each other, for the measurement we have to select one pixel to determine the direction as the viewing direction in Figure 6. Since the OSC in Section 2 is optimized to realize the FV camera. The direction of OSC is inappropriate for the measurement of ζ, ζ' . We determine the viewing direction from the FOE point on the image. ‘‘FOE’’, standing for ‘‘Focus Of Extension’’, is the point on the image back-projecting to the same object in the real world while zooming. We can measure the coordinates of the FOE on the input image beforehand.

The following shows the concrete method for measuring the gap r .

- (1) Calibrate the camera in one base direction and obtain Ψ for that direction.
- (2) Measure the FOE point in the direction. Mark the object which is back-projected from the FOE as ‘‘Object on FOE’’ (OF).
- (3) Measure the distance l from the rotation center to OF.
- (4) Rotate the camera.
- (5) Record the OF’s coordinates on image.
- (6) Repeat Step 4, 5, and get enough samples.
- (7) Calculate ζ, ζ' for each sample.
- (8) Calculate r from equation (8) for each sample, and get the average as the result of the gap.

3.2 Determination of the Limitation of Sub-range as the FV camera

In Figure 7, ν pixels in a distance of λ from OSC (${}^{\text{im}}O_x, {}^{\text{im}}O_y$) on the image cover an angle of τ . And τ can be calculated by equation (9).

$$\tau = \arctan \left(\frac{\lambda + \nu}{\rho} \right) - \arctan \left(\frac{\lambda}{\rho} \right) \quad (9)$$

Let $\nu = 1$, if the parallax η (Figure 6) is less than τ , it will not be observed at the location of λ from OSC. Figure 8 shows the relation of λ and ζ, ζ' . From Equation (8),(9),(10), we can calculate ζ for a given λ . When λ is larger than the maximum distance on the image from OSC, parallax will be less than one pixel within the image. So ζ for the maximum distance on the image from OSC will be the limitation of the rotary range.

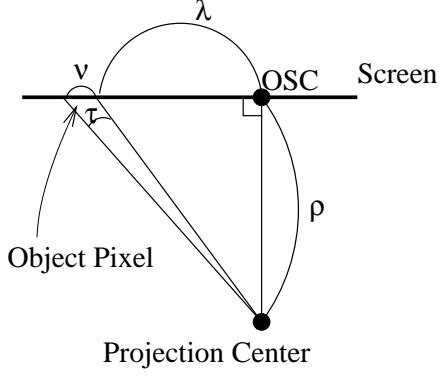


Fig. 7 Angle for Pixels on Image

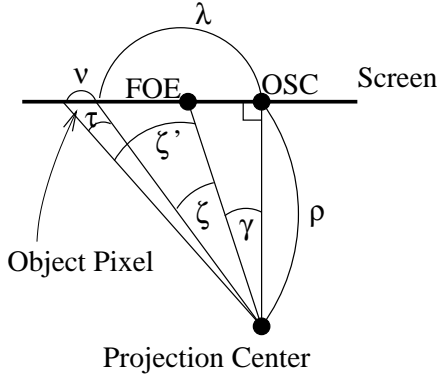


Fig. 8 Limitation for No Parallax Observed

Table 3 Limitation of Rotary Range [deg]

	$\nu = 1$	$\nu = 2$
τ [deg]	0.0477	0.0953
l [cm]		
100	7.981	16.125
200	16.072	33.619
300	24.508	56.032
400	33.558	ALL
500	43.687	ALL
Angle[deg]	21.812	

$$\begin{aligned} \lambda &= \rho \tan(\zeta + \gamma) \\ \lambda + \nu &= \rho \tan(\zeta' + \gamma) \end{aligned} \quad (10)$$

3.3 Experimental Results

Based on the model shown above, we have measured the gap r and derived the limitation ζ shown in Table 3.

The table shows the limitations for several cases. For each case, the distance of the object differs. As shown in Table 3, we measured the limitation for object from about 1m to 5m. Meanwhile, the last row of the table shows the angle of the whole image. As for $\nu = 1, l = 100$, the limitation shown is **7.981**,

Table 4 Errors of Different Parameters

Combination	S	\bar{e} [rad]	\bar{e} [pixel]
Dir(-15), Ψ (-15)	0.000418	0.000651	0.78
Dir(-15), Ψ (-40)	0.000794	0.000882	1.06
Dir(-15), Ψ (-65)	0.000447	0.000671	0.81
Dir(-40), Ψ (-15)	0.000879	0.000932	1.12
Dir(-40), Ψ (-40)	0.000518	0.000718	0.86
Dir(-40), Ψ (-65)	0.001085	0.001037	1.25
Dir(-65), Ψ (-15)	0.000293	0.000553	0.66
Dir(-65), Ψ (-40)	0.000807	0.000960	1.15
Dir(-65), Ψ (-65)	0.000267	0.000527	0.63

less than the angle(**21.812**). This means for the object at 1m, the projection model as the FV camera is inappropriate and the camera should not be considered as the FV camera.

By measuring the gap r , we can determine the limitation of the rotary range for parallax-free. As described at the beginning of this paper, we are able to partition the full rotary range into several sub-ranges and within each of them the PFV camera can be calibrated and used as the FV camera. To realize the FV camera over the *full* rotary range, we have to integrate the calibration processes in all of the sub-ranges. The detailed integration method is described in the next section.

4. Integration of Calibrating Processes Over Full Rotary Range

Given a PFV camera, we are able to calibrate it by the method shown in Section 2 as the FV camera. We also can determine limitation of the sub-range within which we can consider it as the FV camera. To realize the FV camera over the full rotary range, it is reasonable to partition the full range to several such sub-ranges and calibrate the camera for each of them. But if the parameters Ψ for each sub-range is optimized individually, ignoring the physical characteristics of each parameter, the property of the FV camera is not guaranteed to be preserved among all of the sub-ranges. Table 4 shows the evaluation results for different parameters Ψ optimized in different base direction. The error grows greater when using other parameters. For the error in pixel is higher than 1.0, the property of the FV camera is destroyed. So we have to integrate these calibration processes to keep the property.

The integration is based on a controlled optimization of the parameters Ψ . For Ψ has a dimension of 13, the optimal result is a local minimum according to the evaluation function. And not all local minimums match the camera

Table 5 Average of Errors By Applying Controlled Optimization

	(-22)to(-33)		(-47)to(-58)	
	\bar{e} [rad]	\bar{e} [pixel]	\bar{e} [rad]	\bar{e} [pixel]
$\{\Psi\}_c$	0.002356	2.83	0.004994	6.00
$\{\Psi\}$	0.020317	24.42	0.024804	29.81

in practice. By controlling the optimization, we aim to derive Ψ for not only numerically low error but also match the camera in practice.

In Section 2.4.2, optimized values of each parameter for 3 sub-ranges are shown in Table 2. From the table, the focal length(ρ), the parameters about the lens distortion(κ , (dO_x , dO_y)) and the values of the parameter to correct the camera direction (T_{off}), are almost unchanged for each sub-range while others change great. So we determine the optimizing step as the following:

- (1) Only optimize ρ , κ , (dO_x , dO_y) and T_{off} , while keeping the other parameters fixed.
- (2) Keeping ρ , κ , (dO_x , dO_y) and T_{off} as the optimized value, optimize the rest parameters.

For 3 sub-ranges with the base direction as -15 , -40 . -65 in pan, we derive a set of Ψ , noted as $\{\Psi\}_c$ with the controlled optimization. For comparison, we also derive a set $\{\Psi\}$ without any controls. The following experiments are done to estimate the accuracy of each set over the sub-range:

- (1) Acquire 2 pairs of images. One pair are in the direction of -22 and -33 , whose viewing field overlaps each other. The two directions are within the sub-range of -15 and -40 respectively. The other pair are in the direction of -47 and -58 and are within the sub-range of -40 and -65 respectively.
- (2) For both pairs, select multiple related feature points on each image as mentioned in Section 2.3.
- (3) For each pair of related feature point, calculate the error e_c and e defined in equation 6 by applying $\{\Psi\}_c$ and $\{\Psi\}$ respectively, and calculate the average of \bar{e}_c and \bar{e} .

Table 5 shows the experimental results.

From the table, by controlling the optimization for all sub-ranges, the error caused by switching the parameter over sub-ranges is kept within under 10 pixels. The error is about 30 pixels when no controlling. This prove the controlled optimization propose is efficient in

keeping the FV camera property over the sub-ranges.

Moreover, in the above experiment, the initial value of each Ψ for the controlled optimization is given as the the best optimized Ψ for one sub-range. So the total integration method of all calibration processes can be claimed as below:

- (1) Calibrate the camera for each sub-range, without calibration controls.
- (2) Select the best parameter Ψ with lowest error among all the sub-ranges.
- (3) Giving the selected Ψ as the initial value for all of the sub-ranges, optimize each Ψ by applying the controlled step shown above.

The experimental results show that by the integration method, the property of the FV camera is preserved. Totally, we realize the FV camera over the full rotary range by using a PFV camera.

5. Conclusion

In this paper, we describe a calibration method for a PFV camera to utilize it as the FV camera. We propose:

- An accurate projection model which absorbs kinds of distortion.
- A camera work for calibration.
- A method to measure the gap between the projection center and the rotation center.
- An integration method of calibration processes for multiple sub-ranges.

Experimental results prove the effectiveness of the proposed model and methods. Based on the projection model, we succeed in calibrating a PFV camera as the FV camera within a narrow rotary range. By measuring the gap between the projection center and the rotation center, we can determine the limitation of sub-range for considering the PFV as the FV camera. For the full rotary range, we can partition it to multiple sub-ranges to use the PFV as FV camera within each partition. Furthermore, by applying the integration methods for all calibration processes of the sub-ranges, the FV camera can be realized over all sub-ranges. Our proposed methods are efficient for a practical realization of the FV camera.

References

- 1) T.Wada and T.Matsuyama, "Appearance Sphere: Background Model for Pan-Tilt- Zoom Camera", Proc. of 13th ICPR, pp.A-718-A-722, Vienna Austria, Aug. 1996.

- 2) Matsuyama, T. "Cooperative Distributed Vision – Dynamic Integration of Visual Perception, Action, and Communication –," Proc. of Image Understanding Workshop, pp. 365-384, 1998
- 3) Hirotake Yamazoe, Akira Utsumi, Nobuji Tetutani, "Automatic Camera Calibration Method for Multiple Camera Based Human Tracking System," IE2000-173 (2001-02).
- 4) 東海彰吾, 弓場 竜, ウ 小軍, 松山隆司, "アクティブカメラを用いた動的広域シーンの映像提示法," 信学論 (D-II), vol.J84-D-II, no.8, pp.1910-1920, (2001-8).
- 5) ウ 小軍, 和田俊和, 東海彰吾, 松山隆司, "平面間透視投影を用いた並列視体積交差法," 情処論, vol.42 no.SIG6(CVIM 2), (2001-6).
- 6) Z.Zhang, "A Flexible New Technique for Camera Calibration," Proc. ICCV(1999)
- 7) 出口光一郎, 岡谷貴之, "3次元環境理解のための多視点カメラのキャリブレーション," 情処研報 2002-CVIM-131, vol.2002, no.2, pp.1-8, (2002-1).
- 8) 山内結子, 林 正樹, 井上誠喜, 下田 茂, "主点一致型カメラ雲台を用いた全天周大画面画像の作成," 信学技報 IE98-75 (1998-11).